HHS Public Access

Author manuscript

J Comp Neurol. Author manuscript; available in PMC 2018 February 15.

Published in final edited form as:

J Comp Neurol. 2017 February 15; 525(3): 592–609. doi:10.1002/cne.24089.

Three-dimensional synaptic analyses of mitral cell and external tufted cell dendrites in rat olfactory bulb glomeruli

Jennifer N. Bourne[1] and **Nathan E. Schoppa**[1,2]

[1]Department of Physiology and Biophysics, University of Colorado School of Medicine, Aurora, CO 80045, United States

[2]Neuroscience Program, University of Colorado School of Medicine, Aurora, CO 80045, United States

Abstract

Recent studies have suggested that the two excitatory cell classes of the mammalian olfactory bulb, the mitral cells (MCs) and tufted cells (TCs), differ markedly in physiological responses. For example, TCs are more sensitive and broadly tuned to odors than MCs and also are much more sensitive to stimulation of olfactory sensory neurons (OSNs) in bulb slices. To examine the morphological bases for these differences, we performed quantitative ultrastructural analyses of glomeruli in rat olfactory bulb under conditions in which specific cells were labeled with biocytin and 3,3'-diaminobenzidine. Comparisons were made between MCs and external TCs (eTCs), which are a TC sub-type in the glomerular layer with large direct OSN signals and capable of mediating feedforward excitation of MCs. Three-dimensional analysis of labeled apical dendrites under an electron microscope revealed that MCs and eTCs in fact have similar densities of several chemical synapse types including OSN inputs. OSN synapses also were distributed similarly, favoring a distal localization on both cells. Analysis of unlabeled putative MC dendrites further revealed gap junctions distributed uniformly along the apical dendrite, and, on average, proximal with respect to OSN synapses. Our results suggest that the greater sensitivity of eTCs versus MCs is not due to OSN synapse number or absolute location but rather a conductance in the MC dendrite that is well-positioned to attenuate excitatory signals passing to the cell soma. Functionally, such a mechanism could enable rapid and dynamic control of OSN-driven action potential firing in MCs through changes in gap junction properties.

Graphical abstract

Corresponding Author: Nathan E. Schoppa, Ph.D., University of Colorado School of Medicine, 12800 East 19th Ave., Rm. P18-7115, Aurora, CO 80045, Phone: (303) 724-4523, Fax: (303) 724-4501, Nathan.Schoppa@ucdenver.edu.

Conflict of Interest Statement: The authors have no conflict of interest with studies described in this manuscript.

Role of Authors: JNB and NES had full access to all of the data in the study and take responsibility for the integrity of the data and the accuracy of the data analysis. Study concept and design: JNB and NES. Acquisition of data: JNB. Analysis and interpretation of data: JNB and NES. Drafting of the manuscript: JNB and NES. Critical revision of the manuscript for important intellectual content: JNB and NES. Statistical analysis: JNB and NES. Obtained funding: NES.

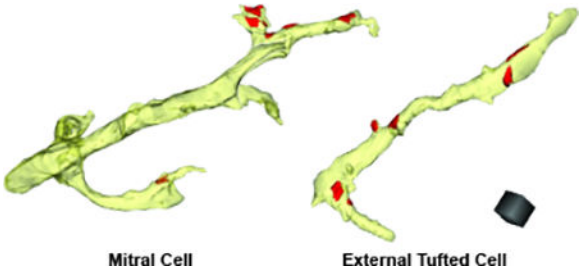

Using quantitative ultrastructural analyses, the authors show that two excitatory cell types of the olfactory bulb, mitral cells and external tufted cells, have similar densities of sensory neuron inputs on apical dendrites. Differences in physiological responses of these two cells are instead likely due to well-positioned dendritic gap junctions.

Keywords

olfaction; glomerulus; serial section electron microscopy; gap junctions; reconstructions; sensory neuron; RRID:SCR_002716

Introduction

Within the mammalian olfactory bulb, olfactory sensory neurons (OSNs) transmit information onto output mitral cells (MCs) and various subpopulations of tufted cells (TCs) that differ in location of their cell bodies and arborization (Macrides and Schneider, 1982; Orona et al., 1984; Schoenfeld et al., 1985; Antal et al., 2006; Imai, 2014). Recent physiological studies have suggested that MCs and TCs in fact have quite distinct odor-evoked responses. As compared to TCs, MCs are less sensitive to odors, more odor-selective, and display significantly delayed action potentials (spikes; Nagayama et al., 2004, Igarishi et al., 2012, Fukunaga et al., 2012; Otazu et al., 2015). Differences have also been observed in synaptic responses in brain slice experiments. For example, in response to stimulation of OSNs at a given intensity, MCs display much weaker somatic current and voltage responses with the rapid time-course expected for direct OSN-to-MC transmission (De Saint Jan et al., 2009; Najac et al., 2011; Gire et al., 2012; Burton and Urban, 2014; Vaaga and Westbrook, 2016). MCs also have much smaller optogenetically-evoked currents that are insensitive to the sodium channel blocker tetrodotoxin (Gire et al., 2012), often used to assay monosynaptic excitation (Petreanu et al., 2009). Amongst TCs, the largest direct OSN currents appear to be in superficial TCs, a class of output cells with cell bodies in the outer external plexiform layer, and external TCs (eTCs), which are glutamatergic interneurons in the glomerular layer that lack lateral dendrites. The difference in synaptic responses between MCs and eTCs also extends to inhibitory synapses, as eTCs have substantially larger inhibitory currents that reflect inputs from glomerular layer interneurons in direct comparisons (Gire and Schoppa, 2009; Whitesell et al., 2013; Banerjee et al., 2015).

At an ultrastructural level, very little is known about the synaptic organization of MC and TC apical dendrites that could give rise to the different physiological responses. One

limitation has been that the vast majority of ultrastructural studies of OSN synapses have not differentiated whether the post-synaptic dendrites were from MCs or TCs (Pinching and Powell, 1971, White, 1972, Hinds and Hinds, 1976, Kasowski et al., 1999). Thus, simple issues such as the number of OSN synaptic contacts onto MCs (Kosaka et al., 2001; Najac et al., 2011) or TCs have never been addressed. A dendrite's complement of ion channels can also impact the size of synaptic signals at the cell soma as reflected in both current and voltage measurements (Rall, 1967; Williams and Mitchell, 2008). In this context, it is interesting that MCs have a large (~1 nS) gap junctional conductance in their apical dendritic tufts (Schoppa and Westbrook, 2002; Christie et al., 2005; Pimental and Margrie, 2008; Maher et al., 2009) that is present at a much lower level in eTCs (Hayar et al., 2005; Gire et al., 2012). Furthermore, knock-out (KO) of the gap junction protein connexin (Cx) 36 results in the emergence of large direct OSN currents in MCs and rapid spiking (Gire et al., 2012). However, the distribution of gap junctions in MC apical dendrites is not known.

Here we conducted ultrastructural analyses to understand the synaptic organization of the apical dendrites of MCs and eTCs. eTCs, and not other TC subtypes, were chosen for the analysis due to their much larger monosynaptic OSN current versus MCs in pair-cell recordings (Gire et. al., 2012; Vaaga and Westbrook, 2016) and large inhibitory synaptic currents. eTCs can also mediate feedforward excitation of MCs (OSN-to-eTC-to-MC; De Saint Jan et al., 2009; Najac et al., 2011; Gire et al., 2012), and so their comparative synaptic organization versus that of MCs will likely contribute to whether MCs are excited via eTCs or directly by OSNs. We labeled MCs and eTCs in olfactory bulb slices with biocytin, which was then converted into an electron dense substrate using an avidin-biotin complex and 3,3'-diaminobenzidine (DAB). Serial section electron microscopy was used to create 3-dimensional reconstructions of DAB-labeled MC and eTC dendrites where the density and distribution of OSN synapses as well as other chemical synapse types could be quantified. In addition, in a population of unlabeled putative MC dendrites, we examined the distribution of gap junctions and their spatial relationship with respect to OSN synapses and presynaptic sites of neurotransmitter release.

Materials and Methods

Cell Labeling in Olfactory Bulb Slices

Horizontal olfactory bulb slices (330-μm thickness) were prepared from 3 young Sprague Dawley rats (postnatal P8–14; male and female) following general isofluorane anesthesia and decapitation. Slices were then transferred to a recording chamber with oxygenated (95% O_2, 5% CO_2) extracellular solution containing (in mM): 125 NaCl, 25 $NaHCO_3$, 1.25 NaH_2PO_4, 25 glucose, 3 KCl, 2 $CaCl_2$, 1 $MgCl_2$ (pH = 7.3). Patch pipettes for whole-cell fills contained (in mM): 125 K-gluconate, 2 $MgCl_2$, 0.025 $CaCl_2$, 1 EGTA, 2 NaATP, 0.5 NaGTP, 10 HEPES (pH 7.3 with KOH), and biocytin (1%). Intracellular solutions were supplemented with 100 μM Alexa 488 dye (Invitrogen) to establish cellular morphology during the fills.

Olfactory bulb slices were visualized on an upright fluorescence microscope (Zeiss Axioskop) equipped with DIC optics. MCs and eTCs were patched and allowed to fill for 10–15 minutes. Patch pipettes were then gently removed from the cell body, allowing the

membrane to re-seal. All cell-fills were performed between 32 and 35°C. Once cells with intact dendritic arbors had been filled in a given slice, slices were fixed overnight at 4°C in 1% paraformaldehyde and 2.5% glutaraldehyde in 0.1 M phosphate buffer (pH 7.4).

The next day, slices were rinsed in 0.1 M phosphate buffer and incubated in a 3% H_2O_2 solution for 30 minutes. The tissue was then cryoprotected in increasing concentrations of sucrose solution (10%/20%/30%) and freeze/thawed in liquid nitrogen 5–6 times. Slices were incubated in 1% ABC Solution (Vectastain Elite ABC kit, Vector Labs) at room temperature for 1 hour and then overnight at 4°C. After rinsing the tissue in 0.1 M phosphate buffer, slices were incubated in a 1% 3,3'-diaminobenzidine (DAB) solution for 30 minutes before 3% H_2O_2 was added to catalyze the reaction. Once cells filled with biocytin turned brown/black (30–60 seconds), the reaction was stopped by transferring the slices back to 0.1 M phosphate buffer (Figure 1A).

Electron Microscopy

Slices were embedded in 5% agarose in 0.1 M phosphate buffer and sliced on a vibratome into 80-μm-thick sections. The 80-μm vibraslices containing the DAB labeled processes were rinsed in 100 mM cacodylate buffer and then immersed in 1% osmium and 1.5% potassium ferrocyanide for 15 min, rinsed five times in cacodylate buffer, immersed in 1% osmium for 1 hour (Figure 1B), and then rinsed five times for 2 min each in buffer and two times briefly in water. Slices were then transferred to graded ethanols (50, 70, 90, and 100%) containing 2% uranyl acetate for 15 minutes each. Finally, slices were transferred through propylene oxide at room temperature and then embedded in LX112 and cured for 48 h at 60°C in an oven (modified from Harris et al., 2006).

Serial sections (50-nm thickness) were cut from a small trapezoid positioned over glomeruli with DAB-labeled dendrites and were picked up on Formvar-coated slot grids (EMS). Sections were imaged either on a FEI Tecnai G2 transmission electron microscope at 80 kV with a Gatan UltraScan 1000 digital camera at a magnification of 4,800× or a Zeiss SUPRA 40 field-emission scanning electron microscope (FE-SEM) equipped with an integrated module called ATLAS™ (Automated Large Area Scanning; software version 3.5.2.385; Kuwajima et al., 2013).

Image Analysis and 3-D Reconstruction

The serial section images were aligned and dendrites were traced using the RECONSTRUCT™ software (http://synapses.clm.utexas.edu/tools/reconstruct/reconstruct.stm, RRID:SCR_002716; Fiala and Harris, 2001; Fiala, 2005). Individual dendritic branches were treated as unique segments. A segment had to be at least 3 μm in length, 0.3 μm in diameter, and have one synapse to be included in most of the analyses. Terminal ends of dendrites were defined as a segment that tapered and disappeared through serial sections. Axons were characterized by small caliber projections that would swell to form *en passant* boutons that contained synaptic vesicles and formed synapses. Putative excitatory and inhibitory synapses and OSN synapses onto DAB-labeled MC and eTC dendrites were categorized based on their ultrastructural appearance as described in the Results. In studies of unlabeled dendrites on putative MCs, OSN synapses were identified

based on their asymmetric appearance and the dark, granular appearance of the presynaptic axon terminals (Pinching and Powell, 1971; Kasowski et al., 1999). The putative excitatory presynaptic release sites were identified based on their presence at asymmetric synapses and the appearance of clear, round vesicles. Gap junctions were identified through serial sections by the dark, dense staining plaques between adjacent dendritic membranes (Brightman and Reese, 1969; Kosaka and Kosaka, 2004). That the unlabeled processes were dendrites (versus axons) was determined by their greater diameter, more uniform size as a function of length, the presence of fewer synaptic vesicles, and the fact that they formed both afferent and efferent synapses.

In the analysis of the gap junctionally or synaptically connected partners of unlabeled putative MC dendrites (Figure 6), the identity of the partner dendrites (putative excitatory versus inhibitory) was determined by following these dendrites to where they formed an asymmetric or symmetric synapse onto another (third) dendrite. Identifying a specific dendrodendritic synapse to be asymmetric, with a clear post-synaptic density that differed in thickness from the presynaptic membrane, was more difficult than for axodendritic synapses (see red arrow in Figure 1F) and generally required imaging across multiple sections.

Synapse size was calculated by summing the product of active zone length, as determined by a darker, slightly fuzzy thickening of the presynaptic membrane (Figure 1E,F), and section thickness over the number of sections in which they appear. Dendrite lengths, distances of synapses, gap junctions, and release sites from distal ends of dendrites, and distances between these elements were measured across serial sections using the z-trace tool in RECONSTRUCT™.

Statistical Analyses

Data were graphed and statistically analyzed using Excel. Results are presented as mean ± SEM and include the relevant *n* values for each analysis. One-way ANOVAs were used to analyze the effect of distance from the distal end of dendritic segments on synaptic, gap junction, and release site densities, followed by post-hoc two-tailed Student's *t* tests. The two-sample Kolmogorov-Smirnov test was used to compare cumulative distributions that reflected distances from distal end of dendrites for various elements, separation between the elements, and synapse size. Remaining analyses were performed using two-tailed Student's *t* tests where appropriate.

Results

Individual MCs and eTCs were filled with Alexa 488 (100 μM) and biocytin (1%) during whole-cell patch-clamp recordings in olfactory bulb slices from juvenile rats (P8–14). MCs were identified by their characteristic row of large cell bodies, while eTCs were identified by their juxtaglomerular position, large, spindle-shaped cell bodies, lack of secondary dendrites, as well as their large apical dendritic tufts that occupied most of an adjacent glomerulus (Macrides and Schneider, 1982; Hayar et al., 2004). Following incubation with an avidin-biotin complex, tissue was reacted with DAB to form an electron dense substrate (see MC example in Figure 1A,B) and then processed for electron microscopy.

Basic characterization of DAB-labeled dendrites and synapses

Serial sections (50–150 sections; 50-nm thickness) of glomeruli containing DAB-labeled MC or eTC dendrites were cut and imaged on a transmission electron microscope. Images of the dendrites and their synapses were then aligned, traced and reconstructed. Dendritic segments from both MCs (Figure 1C) and eTCs (Figure 1D) varied in length and synaptic density. Thirteen dendritic segments from two labeled MCs ranged in length from 4.1 to 34.8 μm with overall synaptic densities that ranged from 0.16 to 1.38 synapses (syn)/μm. Ten dendrites from two labeled eTC cells ranged in length from 3.5 to 22.2 μm and had synaptic densities varying from 0.29 to 1.12 syn/μm. The two example cells representing MCs or eTCs did not differ in the length of their reconstructed segments ($p \geq 0.12$) nor their total synaptic density ($p \geq 0.52$), and so their data for each cell-type were pooled. The average lengths of the dendritic segments sampled were similar for MCs versus eTCs (MC: 11.2 ± 2.1 μm; eTC: 8.6 ± 1.4 μm; $p = 0.38$). Dendrites from eTCs were more likely to be branched than MC dendrites (83% of eTC dendrites vs 30% of MC dendrites).

The categorization of synapses onto the DAB-labeled dendrites was complicated by the fact that the DAB precipitate obscured possible postsynaptic densities. This made it difficult to determine whether the synapses were asymmetric or symmetric, which is one of the ultrastructural criteria typically used to distinguish putative excitatory versus inhibitory synapses (Gray, 1959; Colonnier, 1968). Instead, we defined a synapse onto labeled dendrites to be “putative excitatory” if it had round, clear vesicles at the presynaptic membrane (Figure 1E). Additionally, when the processes containing these presynaptic elements were followed, they formed asymmetric synapses onto unlabeled dendrites (see Figures 1F, red arrow, and 6Aii for examples of asymmetric synapses). Similarly, “putative inhibitory” synapses had pleomorphic, flattened vesicles (Figure 1F), and their associated processes formed symmetric synapses onto unlabeled dendrites (see Figure 6B2 for example of symmetric synapse). These methods for categorizing synapses assumed that an individual process making synapses onto the DAB-labeled dendrite was homotypic for possible functional type (either excitatory or inhibitory), but this was generally reasonable given available data. Both putative excitatory and inhibitory synapses were intermingled on the dendritic segments from MCs (Figure 1C) and eTCs (Figure 1D).

The large majority of putative excitatory synapses were formed directly onto the dendritic shafts of both cell types (90% of synapses on MCs, 92% of synapses on eTCs), although examples on spine-like protrusions were also observed (Figure 1G,H). All of the putative excitatory synapses on the spine-like protrusions had the ultrastructural characteristics of OSN synapses (see below). Spine-like protrusions were characterized by a bulbous head, some extending small membranous projections, and a narrower neck that connected back to the dendritic shaft. Unlike typical dendritic spines in the cortex or hippocampus (Bourne and Harris, 2008), the synapses were usually not on the end of the spine-like protrusions. Putative inhibitory synapses were always on the dendritic shaft. In addition, both MC and eTC dendrites had non-synaptic filopodia-like structures that were long (>0.5 μm), thin projections arising from the dendritic shaft (Figure 1G,H), although they were more common on MCs (46% of MC dendrites vs 20% of eTC dendrites).

Our analysis of the apical dendrites of MCs and eTCs focused on the ultrastructure of dendrites in the glomerular tuft and did not examine properties of the apical dendritic trunk. Prior dendritic patch recordings (Urban and Sakmann, 2002) indicated that the relatively long trunk of the MC apical dendrite attenuates excitatory synaptic signals that originate in the tuft only modestly, about 30–40%, as they pass to the MC soma. This implies that a difference in trunk length or ultrastructure does not contribute significantly to the physiological phenomena that motivated our studies, including the much smaller glomerular synaptic signals recorded in MCs versus eTCs.

Subtypes of putative excitatory synapses

In electron micrographs, the *en passant* boutons associated with presynaptic axon terminals of OSNs are characterized by a dark, granular appearance and contain a large number of round, clear vesicles (Pinching and Powell, 1971; Kasowski et al., 1999). The DAB-labeled dendrites of both MCs and eTCs displayed numerous OSN contacts by these criteria (Figure 2A,B; MC: 43 OSN synapses across 13 dendritic segments; eTC: 26 OSN synapses across 10 dendritic segments), and the overall OSN synaptic density was similar in the two cell-types (Figure 2C; MC: 0.32 ± 0.06 syn/μm; eTC: 0.34 ± 0.04 syn/μm; $p = 0.82$). The lengths of the dendritic segments that were analyzed varied considerably (see above), but we observed no correlation between segment length and the OSN synapse density estimate derived from each segment ($R^2 = 0.05$; Figure 2D). In addition, synapse size can be correlated with synaptic strength (Harris and Stevens, 1989, Schikorski and Stevens, 1997, Bartol et al., 2015), but we found no difference in the areas of OSN synapses between MCs and eTCs (Figure 2E; K–S test: $p = 0.63$).

Both cell types also displayed presynaptic axon terminals that lacked the characteristic dark appearance of OSN axons but still had the round, clear vesicles consistent with excitatory synapses (Figure 2B, orange arrows; see also orange synapses/arrows in Figure 1C,D). There was a trend for the synaptic density of the unidentified axonal inputs to be higher in eTCs versus MCs (Figure 2C), but the difference was not significant across our samples (MC: 4 synapses across 13 dendritic segments, density = 0.04 ± 0.02 syn/μm; eTC: 9 synapses across 10 dendritic segments, density = 0.13 ± 0.04 syn/μm; $p = 0.12$). Combining all axonal inputs revealed that the overall density of these synapses was not significantly different between MCs and eTCs (Figure 2C; 0.36 ± 0.07 syn/μm for MCs; 0.47 ± 0.05 syn/μm for eTCs; $p = 0.30$). Interestingly, both cell types displayed a single example that appeared to be an incoming excitatory dendrodendritic synapse (not shown). These numbers for putative excitatory dendrodendritic synapses onto MC/eTC dendrites correspond to a density of only ~0.01 syn/μm.

In addition to the density of synapses, the position of excitatory synapses on a cell's dendritic arbor can impact the size of the excitatory signal at the cell body (Rall, 1967; Williams and Mitchell, 2008). The distal/proximal orientation of the dendrites was tracked on low magnification images by their position within the glomerulus relative to the main trunk of the apical dendrite of the labeled neuron. To analyze the distribution of OSN synapses on MCs and eTCs, dendritic segments at least 6 μm in length were selected and broken down into 2-μm intervals beginning at the most distal end of the reconstructed

segments (Figure 3A). On MCs, the density of OSN synapses was highest at the distal-most 2 μm of the dendritic segments and decreased with distance from the distal end (Figure 3B; $n = 12$ segments, $F_{(5,56)} = 3.19$, $p = 0.013$). In most of the MC segments analyzed, we were unable to determine definitively whether the distal-most 2 μm reflected the terminal ends of dendritic branches. However, in four additional short MC dendritic segments that were definitively determined to be at the terminal end (see Methods), we always observed 1–2 OSN synapses within 0.5 μm of the ends (Figure 3F). Thus, OSN synapses were preferentially located at distal ends of MC apical dendrites. On dendritic segments of eTCs, the distribution of OSN synapses did not significantly vary with distance when the dendritic segments were analyzed in 2-μm intervals (Figure 3C; $n = 7$ dendrites, $F_{(5,28)} = 1.87$, $p = 0.13$). However, to account for the lower sample size for eTCs, we also analyzed the dendritic segments in longer section-intervals, comparing the densities between 0–4 μm and 4–10 μm. In this analysis, eTCs as well as MCs displayed higher OSN synapse densities in the distal-most 4 microns of the dendritic segments (Figure 3B,C (insets); eTCs: 0–4 μm = 0.46 ± 0.12 syn/μm, 4–10 μm = 0.19 ± 0.06 syn/μm, $p = 0.046$; MCs: 0–4 μm = 0.52 ± 0.12 syn/μm, 4–10 μm = 0.23 ± 0.09 syn/μm, $p = 0.028$). We also determined the distribution of distances from OSN synapses to the distal end of the dendritic segments (Figure 3D) and found no difference between MCs and eTCs (K–S test: $p = 0.46$; pooled distance measurements from MC or eTC dendrites ≥ 8 μm; 34 MC synapses, 18 eTC synapses).

Interestingly, MCs displayed evidence for clustering of OSN synapses. This was evident in many example segments (Figure 1C,D; Figure 3A) and in plots of nearest neighbor distances between synapses (Figure 3E). For MCs, most OSN synapses (~75%) had a nearest neighbor within ~1.2 μm, and the distributions did not appear to follow the single exponential function expected if the synapses were distributed by a single random Poisson process. In eTCs, some OSN synapses were within ~1 μm of each other (Fig. 3A,D), although whether these reflected a distinct clustering process was not clear. Between MCs and eTCs, the distributions of nearest-neighbor distances for OSN synapses were not significantly different (K–S test: $p = 0.084$).

Subtypes of putative inhibitory synapses

Amongst putative inhibitory synapses terminating on the DAB-labeled processes, most appeared to be dendrodendritic rather than axonal in both MCs and eTCs (Figure 4A; MCs: 11 dendrodendritic, 2 axonal across 13 dendritic segments; eTCs: 9 dendrodendritic, 1 axonal across 10 dendritic segments). The density of all putative inhibitory synapses (dendrodendritic plus axonal) did not differ between MCs and eTCs (Figure 4B; 0.10 ± 0.03 syn/μm for MCs, 0.15 ± 0.02 syn/μm for eTCs, $p = 0.28$), although there were significantly fewer of them versus putative excitatory synapses for both cell types ($p \leq 0.0019$). We also calculated the synaptic area for the putative inhibitory synapses (all subtypes), finding that they were somewhat smaller than putative excitatory synapses for MCs (Figure 4C; excitatory: 0.11 ± 0.01 μm^2, $n = 48$; inhibitory: 0.060 ± 0.010 μm^2, $n = 13$; $p = 0.011$) and eTCs (excitatory: 0.12 ± 0.01 μm^2, $n = 36$; inhibitory: 0.077 ± 0.007 μm^2, $n = 10$; $p = 0.020$). The putative inhibitory synapses were similar in size to axodendritic synapses found in regions such as area CA1 of the developing hippocampus (Watson et al., 2015) and lateral amygdala (Ostroff et al., 2010). Finally, we analyzed the distribution of putative inhibitory

synapses along MC and eTC dendrites and did not observe a significant pattern in their localization along dendrites of either cell type (Figure 4D,E; density comparisons between 0–4 μm and 4–10 μm: $p = 0.45$ for MC, $p = 0.12$ for eTCs).

Distribution of OSN synapses, gap junctions, and release sites on unlabeled dendrites

Previous studies in Cx36 KO mice suggested that direct OSN synaptic signals may be strongly attenuated by gap junctions that occur at a much higher density on the apical dendrites of MCs versus eTCs (Gire et al., 2012). For analyzing the distribution of gap junctions on MCs, we had difficulty identifying them in our DAB-labeled dendrites, and so we instead examined unlabeled dendritic segments in the same slices that appeared to be excitatory and that included gap junctions. We categorized these processes as putative MC dendrites since MCs display a 10–30-fold larger gap junctional conductance than eTCs (Hayar et. al., 2005; Gire et al., 2012). A subset of the gap junction-containing dendrites could have reflected eTCs or other classes of TCs, but we considered that their classification as putative MC dendrites was reasonable given available data. The segments reflected the dendrites of MCs or TCs, and not inhibitory cells, based on the presence of round, clear vesicles and their formation of asymmetric synapses onto the dendrites of other cells. Gap junctions were identified by the appearance of dense staining plaques between two adjoining dendritic membranes (Brightman and Reese, 1969; Kosaka and Kosaka, 2004; Figure 5A,B).

Within the putative MC dendritic segments that were ≥6 μm in length (examples in Figure 5C), we found that OSN synaptic density was highest on the distal-most 2 μm of the segments and decreased with distance from the end (13 segments; $F_{(4,46)} = 3.1$, $p = 0.023$; Figure 5D), similar to what was observed in DAB-labeled MCs (Figure 3B). Gap junctions (overall density = 0.28 ± 0.4/μm), however, appeared to have a much more uniform distribution with no significant differences in density between distal and proximal ends ($F_{(4,46)} = 0.35$, $p = 0.84$; Figure 5D). Similarly, the position of the gap junctions on the dendritic segments was more proximal than OSN synapses, as reflected in the distributions of distances from the distal end (K–S: $p = 0.005$; pooled data from all putative MC dendrites ≥ 8 μm; 30 OSN synapses, 18 gap junctions; Figure 5E). We also measured the distances between OSN synapses and gap junctions (Figure 5F). As was observed in the DAB-labeled MC dendritic segments, a large fraction of the OSN synapses in the putative MC segments were clustered together, within 1–2 μm of each other, but OSN synapses were significantly farther from gap junctions (K–S test, OSN-OSN vs OSN-GJ distribution; $p = 0.002$). Thus gap junctions were not co-clustered with OSN synapses.

Within the unlabeled dendritic segments of putative MCs, we also observed numerous presynaptic vesicular release sites that appeared to be excitatory (overall density = 0.19 ± 0.02 release sites/μm across 13 dendritic segments). These were indicated by the presence of docked round, clear vesicles positioned across a synaptic cleft from a postsynaptic density (Figure 5B, green arrow; Pinching and Powell, 1971). By activating other excitatory and GABAergic cells at a glomerulus, neurotransmitter released from these sites can modulate MC/TC activity downstream of OSN inputs. Interestingly, the density of these release sites increased from distal to more proximal regions of the dendrites (Figure 5D; $F_{(4,46)} = 3.6$, $p = 0.012$), differing from both the distal-favoring OSN synapses and evenly-distributed gap

junctions. The positioning of release sites and OSN synapses with respect to the distal end of the unlabeled dendritic segments also differed significantly (K–S: $p = 0.0005$; 30 OSN synapses, 17 release sites; Figure 5E). In terms of the distances between individual elements, presynaptic release sites were farther from OSN synapses than OSN synapses were to each other (K–S test, OSN-OSN vs OSN-RS; $p = 0.001$; Figure 5F), indicating that the release sites were not co-clustered with OSNs. The release sites however were much closer to gap junctions (K–S test, OSN-RS vs GJ-RS; $p = 0.006$). The mean separation between a release site and the nearest gap junction in fact was only 1.1 ± 0.2 μm ($n = 25$). Thus, gap junctions and presynaptic release sites on putative MC dendrites were clustered together.

The electrically and chemically-coupled partners of the gap junction-containing, putative MC dendrites were mostly identified (Figure 6). This was done by finding dendrites that were either gap junctionally (Figure 6A) or synaptically (Figure 6B) connected to the putative MC dendrite and following these dendrites to where they formed either an asymmetric or symmetric synapse onto another (third) dendrite. By these criteria, most (78%) of the dendrites that shared a gap junction with the putative MC dendrites appeared to be excitatory while 21% were likely inhibitory (Figure 6C). In contrast, only 15% ($n = 4$) of the dendrites that received a chemical synapse from putative MC dendrites were apparently excitatory while 82% ($n = 21$) were likely inhibitory (Figure 6D). The estimated density of synapses from putative MC dendrites onto other putative excitatory dendrites from this analysis was ~0.03 syn/μm, a quite low value for dendrodendritic synapses between excitatory elements that was roughly similar to that found in the analysis of DAB-labeled dendrites above (~0.01 syn/μm).

There is evidence that OSN synapses occur within an “axonal compartment” located around the outer perimeter of glomeruli (Kasowski et al., 1999; but see Kosaka et al., 2001). Therefore, we wanted also to explore the distribution of OSN synapses and gap junctions relative to position within a glomerulus. An edge of the glomerulus was overlaid with a 12 × 10 × 2 μm grid that was divided into 2 × 10 × 2 μm rectangular cuboids that ran parallel with respect to the glomerular edge (Fig. 7A,B; grid shown in two dimensions). Within each 2 × 10 × 2 μm rectangular cuboid, we counted the number of OSN synapses and gap junctions within putative MC dendrites ($n = 49$ OSN synapses, 26 gap junctions), and divided those values by the summed volume of analyzed dendrites in each cuboid (Figure 7C) to obtain density estimates for dendritic volumes (Figure 7D). We found that OSN synapse densities were highest within 6 μm from the edge of the glomerulus, while gap junctions displayed a much more uniform distribution. These findings support the presence of an outer axonal compartment in glomeruli and also are consistent with data presented earlier indicating that OSN synapses onto MC dendrites are primarily localized to more distal portions of dendrites (Figures 3B, 5D,E) and that gap junctions maintain a more uniform distribution (Figure 5D,E).

Discussion

Recent studies have provided evidence that MCs and TCs have markedly different odor-evoked and synaptic responses. To understand the anatomical bases for the physiological results, we have performed the first quantitative ultrastructural analysis of the synaptic

organization within the glomerulus under conditions in which definitive information was available through biocytin and DAB-labeling about whether observed dendritic elements reflected MCs versus a class of TCs known as external TCs (eTCs). We also analyzed a large sample of unlabeled putative MC dendrites to obtain information about some cellular features that could not be readily visualized in the DAB-labeled processes. Our main results were: (1) OSNs and eTCs had similar densities of OSN synapses as well as other types of chemical synapses; (2) OSN synapses were preferentially localized on distal portions of the apical dendrites on both MCs and eTCs; (3) Gap junctions had a uniform spatial distribution on putative MC dendrites and on average were more proximally located than OSN synapses; and (4) Gap junctions on putative MC dendrites were clustered with presynaptic vesicular release sites. We discuss our ultrastructural findings with respect to observed differences in physiological responses of MCs versus eTCs, as well as other aspects of glomerular signaling.

What explains the difference in direct OSN signal size in MCs versus eTCs?

In responses to both electrical and optogenetic stimulation of OSNs, eTCs display excitatory post-synaptic currents (EPSCs) that reflect direct OSN inputs (“OSN-EPSCs”) that are much larger than in MCs (Gire et al., 2012; Vaaga and Westbrook, 2016). Exactly how much larger OSN-EPSCs are in eTCs may depend on OSN stimulation intensity (Najac et al., 2011; Vaaga and Westbrook, 2016), with estimates ranging from a factor of 30 for weak stimuli (Gire et al., 2012) to a factor of ~4 for strong stimuli (Vaaga and Westbrook, 2016). Certainly the simplest explanation for the large differences in OSN-EPSCs is that OSNs make many more synapses onto the apical dendrites of eTCs versus MCs, but this hypothesis was not supported by our counts of OSN synapses, which showed similar densities on the two cell types (~0.3–0.4 synapses/μm). Moreover, because MCs and eTCs have similar-sized apical dendritic tufts (Macrides and Schneider, 1982), these OSN synapse density estimates imply a similar total number of OSN synapses. In our analysis, we used high electron-density as a marker of OSN axonal boutons, and we did observe putative excitatory axonal boutons that were less electron-dense. Thus, we may have under- or overestimated OSN synapse density depending on the criterion for electron density chosen. Importantly, however, axonal synaptic markers strongly co-localize with the OSN-specific protein olfactory marker protein (OMP; Kasowski et al., 1999; Kim and Greer, 2000), suggesting that most axonal synapses reflect OSNs, and in our experiments OSN synapses were a large fraction (84% across MCs and eTCs) of the total. In addition, MCs and eTCs displayed similar densities when we counted all putative excitatory axonal synapses. Hence, any errors in our estimates of OSN synapse density are likely to be small and cannot account for the large difference in OSN signal size between MCs versus eTCs.

In many neurons, the location of excitatory synapses on the dendritic arbor can also influence the size of current and voltage signals recorded at the cell soma (Rall, 1967; Williams and Mitchell, 2008). Signals from synapses on distal dendrites are especially attenuated by the intracellular resistance and current loss through dendritic conductances. We found that synapse location is in fact likely to be important for explaining the different-sized OSN signals in MCs versus eTCs but only as it relates to a dendritic gap junctional conductance in MCs (Schoppa and Westbrook, 2002, Christie et al., 2005; Kosaka and

Kosaka, 2005; Pimental and Margrie, 2008; Maher et al., 2009) that is present at a much lower level in eTCs (Hayar et al., 2005; Gire et al., 2012). In terms of the absolute positioning of OSN synapses within the apical dendritic tuft, MCs and eTCs displayed no significant difference, but, in unlabeled putative MC dendrites, gap junctions were distributed on average between OSNs and the cell soma. Such a placement could make the gap junctional conductance well-positioned to shunt OSN signals prior to them reaching the cell body of MCs. It should be noted that our results here suggesting that there are no significant differences between MCs and eTCs in the absolute positioning of OSN synapses nor OSN synapse number are in some sense not surprising. Prior studies in Cx36 KO mice showed that eliminating gap junctions causes monosynaptic OSN currents to be very similar in MCs and eTCs (Gire et al., 2012). While KO experiments have their own caveats, those results like our ultrastructural results here suggested that gap junctions and not OSN synapse location or number are the major contributor to the different-sized OSN signals in the two cell-types.

That a dendritic conductance intrinsic to MCs is involved in attenuating OSN signals from distal dendrites of course makes these cells like many neurons throughout the brain (Hoffman et al., 1997; Berger et al., 2001; Williams and Stuart, 2000). An attenuating effect involving gap junctions is however likely to be more complex than that due to other dendritic conductances such as potassium channels. Because at least a major component of the gap junctional conductance is between MC dendrites, the gap junctions would enable sharing of excitatory OSN signals between MCs at the same time that the signal in any one MC is dissipated by current loss. Furthermore, the degree to which a given gap junctional conductance can shunt excitatory inputs on a particular MC will depend on the membrane potential of the dendrites of other MCs with which it is coupled (which will determine the driving force for current flow between dendrites). Interestingly, a modeling study of a gap junctionally-connected network of interneurons in striatum (Hjorth et al., 2009) examined this latter issue, finding that the degree to which gap junctions shunt excitatory inputs decreases as the dendrites of different cells in the network become depolarized by increasingly coincident excitatory inputs.

Other features of the synaptic organization within glomeruli

In our analysis of putative inhibitory synapses on apical dendrites, we found similar densities of dendrodendritic synapses on MCs and eTCs, and, on rare occasions, axonal synapses that appeared to be inhibitory. The similar density of putative inhibitory synapses was somewhat surprising given available physiological evidence. A number of studies that have made side-by-side comparisons between MCs and eTCs have reported that eTCs display much larger GABAergic electrical signals that can be attributed to neurons in the glomerular layer (periglomerular cells or short-axon cells; Gire and Schoppa, 2009; Whitesell et al., 2013; Banerjee et al., 2015). One possible explanation for a small physiological GABAergic signal at the MC soma is that those signals are attenuated by gap junctions in a manner similar to direct OSN signals. With respect to the distribution of putative inhibitory dendrodendritic synapses, we found that they were mixed with presumed excitatory axonal synapses (Kosaka et al., 2001).

Putative excitatory synapses distinct from OSNs were also found on both MCs and eTCs. These included axon terminals that lacked the electron-dense profile of OSN terminals, which most likely reflected centrifugal inputs from olfactory cortex (Pinching and Powell, 1972; Markopoulis et al., 2012; Rothermel and Wachowiak, 2014) and/or cholinergic inputs from the basal forebrain (Kasa et al., 1995; D'Souza and Vijayaraghavan, 2014). Putative excitatory dendrodendritic synapses (Kosaka and Kosaka, 2005) were also observed on both MCs and eTCs, although the estimated density of these synapses (0.01–0.03 syn/μm) was markedly lower than other synaptic elements within glomeruli (e.g., 0.3–0.4 syn/μm for OSN synapses). Additionally, our ultrastructural analysis provided evidence for mixed chemical and electrical signaling (Kosaka and Kosaka, 2005; Hamzei-Sichani et al., 2012; Vivar et al., 2012), as reflected in complexes on putative MC dendrites that contained vesicular release sites and gap junctions in close proximity (<1 μm away). Based on the overall density of release sites (~0.19/μm; see above) and the nearest-neighbor distribution for gap junctions and release sites (Figure 5F), we estimate the density of such complexes to be ~0.12/μm. These mixed complexes are provocative, especially in light of prior evidence that MCs can engage in rapid lateral excitatory interactions at their apical dendrites (Urban and Sakmann, 2002; Schoppa and Westbrook, 2002; Pimental and Margrie, 2008). These interactions, which are AMPA receptor-dependent but abolished in Cx36 KO animals (Christie et al., 2005), do not appear to involve activation of presynaptic autoreceptors on MCs (Pimental and Margrie, 2008) but could involve AMPA receptors on GABAergic interneurons that couple to MCs (see Figure 6B; Kosaka and Kosaka, 2005) or non-synaptic AMPA receptors on other MCs/TCs.

Our ultrastructural analyses revealed one other interesting feature of OSN synapses, perhaps important in synapse development. While we observed that most OSN synapses occurred directly on dendritic shafts (Pinching and Powell, 1971, White, 1972, Hinds and Hinds, 1976), both MCs and eTCs displayed numerous examples of synapses positioned on spine- or filopodia-like structures. One possibility is that these synapses are involved in synaptogenesis. In the hippocampus, where most mature excitatory synapses are on dendritic spines, the progression of synaptogenesis during the first postnatal week has been proposed to involve the extension of dendritic filopodia that then form one or multiple synaptic contacts before retracting back to the dendritic shaft and finally re-emerging as a mature dendritic spine (Fiala et al., 1998; Harris; 1999; Maletic-Savatic et al., 1999). Perhaps MCs and TCs utilize similar mechanisms when forming excitatory synaptic contacts with OSNs, but rather than maturing into a typical dendritic spine, the mature synapses remain on the dendritic shaft. On-going synaptic refinement could also explain the fact that we did not observe a strict segregation of dendrodendritic synapses from OSN axonal synapses (see above), which differed from some previous studies (Kasowski et al., 1999; Kim and Greer, 2000). Our ultrastructural experiments were in rats at postnatal P8–14, when the organization of glomerular synapses may still be in flux (Hinds and Hinds, 1976).

Broader implications

Returning to the issue of direct OSN signal size discussed earlier, our ultrastructural results here have implications that go beyond just explaining why the signals are much smaller in MCs versus eTCs in brain slice recordings. First, the fact that OSN signals at the cell body

are relatively small in MCs itself has immediate functional significance. Because spikes are generally initiated at the MC soma (except when many OSNs are excited simultaneously; Chen et al., 1997), the small direct OSN signal at the soma means that direct OSN inputs will activate MCs with low efficacy. This will be true regardless of the number of OSN-to-MC synapses. Furthermore, because MCs can be activated through a multi-step OSN-to-eTC-to-MC path (De Saint Jan et al., 2009; Najac et al., 2011; Gire et al., 2012), the small direct OSN signal in MCs compared to eTCs means that the system would generally favor multi-step activation of MCs. Multi-step activation of MCs would be all-the-more favored because TCs have greater intrinsic excitability (Liu and Shipley, 2008; Burton and Urban, 2014). In the natural situation, a low efficacy for direct OSN signals in MCs and a preference for multi-step activation could underlie the relatively low sensitivity of MCs to odor as well as their delayed spike responses (Nagayama et al., 2004, Igarishi et al., 2012, Fukunaga et al., 2012; Otazu et al., 2015).

Our results also raise the obvious question: Why do MCs have a significant complement of OSN synapses if their associated signals at the soma are greatly attenuated by dendritic gap junctions? Amongst the possible explanations is that direct OSN synapses in fact drive only local depolarizations that are restricted to the apical dendrites of MCs. These could control functions such as synaptic plasticity. Also, it is possible that the shunting effect of the gap junctions is dynamically modulated, such that direct OSN signals emerge in MCs in certain situations. As discussed above, the shunting capacity of gap junctions may decrease as excitatory inputs are increasingly coincident (Hjorth et al., 2009), as might occur when OSNs at a glomerulus are highly active, or if the gap junctions themselves are down-regulated (Bloomfield and Volgyi, 2009). Importantly, these mechanisms could operate without any change in the number of expressed OSN synapses or gap junctions, enabling rapid changes in the efficacy of direct OSN signals in driving MC spiking.

Acknowledgments

Support: This work was supported by NIH Grant R01 DC006640 (NES).

Other Acknowledgements: We would like to thank Dorothy Dill for her assistance in the Electron Microscopy Core Facility and Dr. Kristen M Harris at the University of Texas at Austin for the use of her Zeiss SUPRA 40 field-emission scanning electron microscope.

Literature Cited

Antal M, Eyre M, Finklea B, Nusser Z. External tufted cells in the main olfactory bulb form two distinct subpopulations. Eur J Neurosci. 2006; 24:1124–1136. [PubMed: 16930438]

Banerjee A, Marbach F, Anselmi F, Koh MS, Davis MB, Garcia da Silva P, Delevich K, Oyibo HK, Gupta P, Li B, Albeanu DF. An interglomerular circuit gates glomerular output and implements gain control in the mouse olfactory bulb. Neuron. 2015; 87:193–207. [PubMed: 26139373]

Bartol TM, Bromer C, Kinney J, Chirillo MA, Bourne JN, Harris KM, Sejnowski TJ. Nanoconnectomic upper bound on the variability of synaptic plasticity. Elife. 2015:e10778. [PubMed: 26618907]

Berger T, Larkum ME, Luscher HR. High I(h) channel density in the distal apical dendrite of layer V pyramidal cells increases bidirectional attenuation of EPSPs. J Neurophysiol. 2001; 85:855–868. [PubMed: 11160518]

Bloomfield SA, Volgyi B. The diverse functional roles and regulation of neuronal gap junctions in the retina. Nat Rev Neurosci. 2009; 10:495–506. [PubMed: 19491906]

Bourne JN, Harris KM. Balancing structure and function at hippocampal dendritic spines. Ann Rev Neurosci. 2008; 31:47–67. [PubMed: 18284372]

Brightman MW, Reese TS. Junctions between intimately apposed cell membranes in the vertebrate brain. J Cell Biol. 1969; 40:648–677. [PubMed: 5765759]

Burton SD, Urban NN. Greater excitability and firing irregularity of tufted cells underlies distinct afferent-evoked activity of olfactory bulb mitral and tufted cells. J Physiol. 592:2097–2118.

Chen WR, Midtgaard J, Shepherd GM. Forward and backward propagation of dendritic impulses and their synaptic control in mitral cells. Science. 1997; 278:463–467. [PubMed: 9334305]

Christie J, Bark C, Hormuzdi S, Helbig I, Monyer H, Westbrook G. Connexin36 Mediates Spike Synchrony in Olfactory Bulb Glomeruli. Neuron. 2005; 46:761–772. [PubMed: 15924862]

Colonnier M. Synaptic patterns on different cell types in the different laminae of the cat visual cortex. An electron microscope study. Brain Res. 1968; 9:268–287. [PubMed: 4175993]

De Saint Jan D, Hirnet D, Westbrook G, Charpak S. External Tufted Cells Drive the Output of Olfactory Bulb Glomeruli. J Neurosci. 2009; 29:2043–2052. [PubMed: 19228958]

D'Souza RD, Vijayaraghavan S. Paying attention to smell: cholinergic signaling in the olfactory bulb. Front Synaptic Neurosci. 2014; 6:21. [PubMed: 25309421]

Fiala JC. Reconstruct: a free editor for serial section microscopy. J Microsc. 2005; 218:52–61. [PubMed: 15817063]

Fiala JC, Feinberg M, Popov V, Harris KM. Synaptogenesis via dendritic filopodia in developing hippocampal area CA1. J Neurosci. 1998; 18:8900–8911. [PubMed: 9786995]

Fiala JC, Harris KM. Extending unbiased stereology of brain ultrastructure to three-dimensional volumes. J Am Med Inform Assoc. 2001; 8:1–16. [PubMed: 11141509]

Fukunaga I, Berning M, Kollo M, Schmaltz A, Schaefer AT. Two distinct channels of olfactory bulb output. Neuron. 2012; 75:320–329. [PubMed: 22841316]

Gire DH, Franks KM, Zak JD, Tanaka KF, Whitesell JD, Mulligan AA, Hen R, Schoppa NE. Mitral cells in the olfactory bulb are mainly excited through a multistep signaling path. J Neurosci. 2012; 32:2964–2975. [PubMed: 22378870]

Gire DH, Schoppa NE. Control of on/off glomerular signaling by a local GABAergic microcircuit in the olfactory bulb. J Neurosci. 2009; 29:13454–13464. [PubMed: 19864558]

Gray EG. Axo-somatic and axo-dendritic synapses of the cerebral cortex: an electron microscope study. J Anat. 1959; 93:345–356.

Hamzei-Sichani F, Davidson KG, Yasumura T, Janssen WG, Wearne SL, Hof PR, Traub RD, Gutierrez R, Ottersen OP, Rash JE. Mixed electrical-chemical synapses in adult rat hippocampus are primarily glutamatergic and coupled by connexin-36. Front Neuroanat. 2012; 6:13. [PubMed: 22615687]

Harris KM. Structure, development, and plasticity of dendritic spines. Curr Opin Neurobiol. 1999; 9:343–348. [PubMed: 10395574]

Harris KM, Perry L, Bourne JN, Feinberg M, Ostroff L, Hurlburt J. Uniform serial sectioning for transmission electron microscopy. Journal of Neuroscience. 2006; 26:12101–12103. [PubMed: 17122034]

Harris KM, Stevens JK. Dendritic spines of CA 1 pyramidal cells in the rat hippocampus: serial electron microscopy with reference to their biophysical characteristics. J Neurosci. 1989; 9:2982–2997. [PubMed: 2769375]

Hayar A, Karnup S, Shipley MT, Ennis M. Olfactory bulb glomeruli: external tufted cells intrinsically burst at theta frequency and are entrained by patterned olfactory input. J Neurosci. 2004; 24:1190–1199. [PubMed: 14762137]

Hayar A, Shipley MT, Ennis M. Olfactory bulb external tufted cells are synchronized by multiple intraglomerular mechanisms. J Neurosci. 2005; 25:8197–8208. [PubMed: 16148227]

Hinds JW, Hinds PL. Synapse formation in the mouse olfactory bulb. I. Quantitative studies. J Comp Neurol. 1976; 169:15–40. [PubMed: 956463]

Hjorth J, Blackwell KT, Kotaleski JH. Gap junctions between striatal fast-spiking interneurons regulate spiking activity and synchronization as a function of cortical activity. J Neurosci. 2009; 29:5276–5286. [PubMed: 19386924]

Hoffman DA, Magee JC, Colbert CM, Johnston D. K+ channel regulation of signal propagation in dendrites of hippocampal pyramidal neurons. Nature. 1997; 387:869–875. [PubMed: 9202119]

Igarashi KI, Idki N, An M, Yamaguchi Y, Nagayama S, Kobayakawa K, Kobayakawa R, Tanifuji M, Sakano H, Chen WR, Mori K. Parallel mitral and tufted cell pathways route distinct odor information to different targets in the olfactory cortex. J Neurosci. 2012; 32:7970–7985. [PubMed: 22674272]

Imai T. Construction of functional neuronal circuitry in the olfactory bulb. Semin Cell Dev Biol. 2014; 35:180–188. [PubMed: 25084319]

Kasa P, Hlavati I, Dobo E, Wolff A, Joo F, Wolff JR. Synaptic and non-synaptic cholinergic innervation of the various types of neurons in the main olfactory bulb of adult rat: immunocytochemistry of choline acetyltransferase. Neuroscience. 1995; 67:667–677. [PubMed: 7675193]

Kasowski H, Kim H, Greer C. Compartmental organization of the olfactory bulb glomerulus. J Comp Neurol. 1999; 407:261–274. [PubMed: 10213094]

Kim H, Greer C. The emergence of compartmental organization in olfactory bulb glomeruli during postnatal development. J Comp Neurol. 2000; 422:297–311. [PubMed: 10842233]

Kosaka K, Aika Y, Toida K, Kosaka T. Structure of intraglomerular dendritic tufts of mitral cells and their contacts with olfactory nerve terminals and calbindin-immunoreactive type 2 periglomerular neurons. J Comp Neurol. 2001; 440:219–235. [PubMed: 11745619]

Kosaka T, Kosaka K. Neuronal gap junctions between intraglomerular mitral/tufted cell dendrites in the mouse main olfactory bulb. Neuroscience Research. 2004; 49:373–378. [PubMed: 15236862]

Kosaka T, Kosaka K. Intraglomerular dendritic link connected by gap junctions and chemical synapses in the mouse main olfactory bulb: Electron microscopic serial section analyses. Neuroscience. 2005; 131:611–625. [PubMed: 15730867]

Kuwajima M, Mendenhall JM, Lindsey LF, Harris KM. Automated transmission-mode scanning electron microscopy (t(SEM) for a large volume analysis at nanoscale resolution. PLoS One. 2013; 8:e59573. [PubMed: 23555711]

Liu S, Shipley MT. Multiple conductances cooperatively regulate spontaneous bursting in mouse olfactory bulb external tufted cells. J Neurosci. 2008; 28:1625–1639. [PubMed: 18272683]

Macrides F, Schneider SP. Laminar organization of mitral and tufted cells in the main olfactory bulb of the adult hamster. J Comp Neurol. 1982; 208:419–430. [PubMed: 7119169]

Maher BJ, McGinley MJ, Westbrook GL. Experience-dependent maturation of the glomerular microcircuit. Proc Natl Acad Sci USA. 2009; 106:16865–16870. [PubMed: 19805387]

Maletic-Savatic M, Malinow R, Svoboda K. Rapid dendritic morphogenesis in CA1 hippocampal dendrites induced by synaptic activity. Science. 1999; 283:1923–1927. [PubMed: 10082466]

Markopoulos F, Rokni D, Gire DH, Murthy VN. Functional properties of cortical feedback projections to the olfactory bulb. Neuron. 2012; 76:1175–1188. [PubMed: 23259952]

Nagayama S, Takahashi YK, Yoshihara Y, Mori K. Mitral and tufted cells differ in the decoding manner of odor maps in the rat olfactory bulb. J Neurophysiol. 2004; 91:2532–2540. [PubMed: 14960563]

Najac M, Jan D, Reguero L, Grandes P, Charpak S. Monosynaptic and Polysynaptic Feed-Forward Inputs to Mitral Cells from Olfactory Sensory Neurons. J Neurosci. 2011; 31:8722–8729. [PubMed: 21677156]

Orona E, Rainer EC, Scott JW. Dendritic and axonal organization of mitral and tufted cells in the ratolfactory bulb. J Comp Neurol. 1984; 226:346–356. [PubMed: 6747027]

Ostroff LE, Cain CK, Bedont J, Monfils MH, Ledoux JE. Fear and safety learning differentially affect synapse size and dendritic translation in the lateral amygdala. Proc Natl Acad Sci USA. 2010; 107:9418–9423. [PubMed: 20439732]

Otazu GH, Chae H, Davis MB, Albeanu DF. Cortical feedback decorrelates olfactory bulb output in awake mice. Neuron. 2015; 86:1461–1477. [PubMed: 26051422]

Petreanu L, Mao T, Sternson SM, Svoboda K. The subcellular organization of neocortical excitatory connections. Nature. 2009; 457:1142–1145. [PubMed: 19151697]

Pimentel D, Margrie T. Glutamatergic transmission and plasticity between olfactory bulb mitral cells. J Physiol (Lond). 2008; 586:2107–2119. [PubMed: 18276730]

Pinching AJ, Powell TP. The neuropil of the glomeruli of the olfactory bulb. J Cell Sci. 1971; 9:347–377. [PubMed: 4108057]

Pinching AJ, Powell TP. The termination of centrifugal fibres in the glomerular layer of the olfactory bulb. J Cell Sci. 1972; 10:621–635. [PubMed: 5038408]

Rall W. Distinguishing theoretical synaptic potentials computed for different soma-dendritic distributions of synaptic input. J Neurophysiol. 1967; 30:1138–1168. [PubMed: 6055351]

Rothermel M, Wachowiak M. Functional imaging of cortical feedback projections to the olfactory bulb. Frontiers in Neural Circuits. 2014; 8:1–14. [PubMed: 24478635]

Schikorski T, Stevens CF. Quantitative ultrastructural analysis of hippocampal excitatory synapses. J Neurosci. 1997; 17:5858–5867. [PubMed: 9221783]

Schoenfeld TA, Marchand JE, Macrides F. Topographic organization of tufted cell axonal projections in the hamster main olfactory bulb: an intrabulbar associational system. J Comp Neurol. 1985; 235:503–518. [PubMed: 2582006]

Schoppa NE, Westbrook GL. AMPA autoreceptors drive correlated spiking in olfactory bulb glomeruli. Nat Neruosci. 2002; 5:1194–1202.

Urban NN, Sakmann B. Reciprocal intraglomerular excitation and intra- and interglomerular lateral inhibition between mouse olfactory bulb mitral cells. J Physiol (Lond). 2002; 542:355–367. [PubMed: 12122137]

Vaaga CE, Westbrook GL. Parallel processing of afferent olfactory sensory information. J Physiol. 2016 Epub ahead of print.

Vivar C, Traub RD, Gutiérrez R. Mixed electrical-chemical transmission between hippocampal mossy fibers and pyramidal cells. Eur J Neurosci. 2012; 35:76–82. [PubMed: 22151275]

Watson DJ, Ostroff L, Cao G, Parker PH, Smith H, Harris KM. LTP enhances synaptogenesis in the developing hippocampus. Hippocampus. 2015; doi: 10.1002/hipo.22536

White EL. Synaptic organization in the olfactory glomerulus of the mouse. Brain Res. 1972; 37:69–80. [PubMed: 4334289]

Whitesell JD, Sorensen KA, Jarvie BC, Hentges ST, Schoppa NE. Interglomerular lateral inhibition targeted on external tufted cells in the olfactory bulb. J Neurosci. 2013; 33:1552–1563. [PubMed: 23345229]

Williams SR, Mitchell SJ. Direct measurement of somatic voltage clamp errors in central neurons. Nat Neurosci. 2008; 11:790–798. [PubMed: 18552844]

Williams SR, Stuart GJ. Site independence of EPSP time course is mediated by dendritic I(h) in neocortical pyramidal cells. J Neurophysiol. 2000; 83:3177–3182. [PubMed: 10805715]

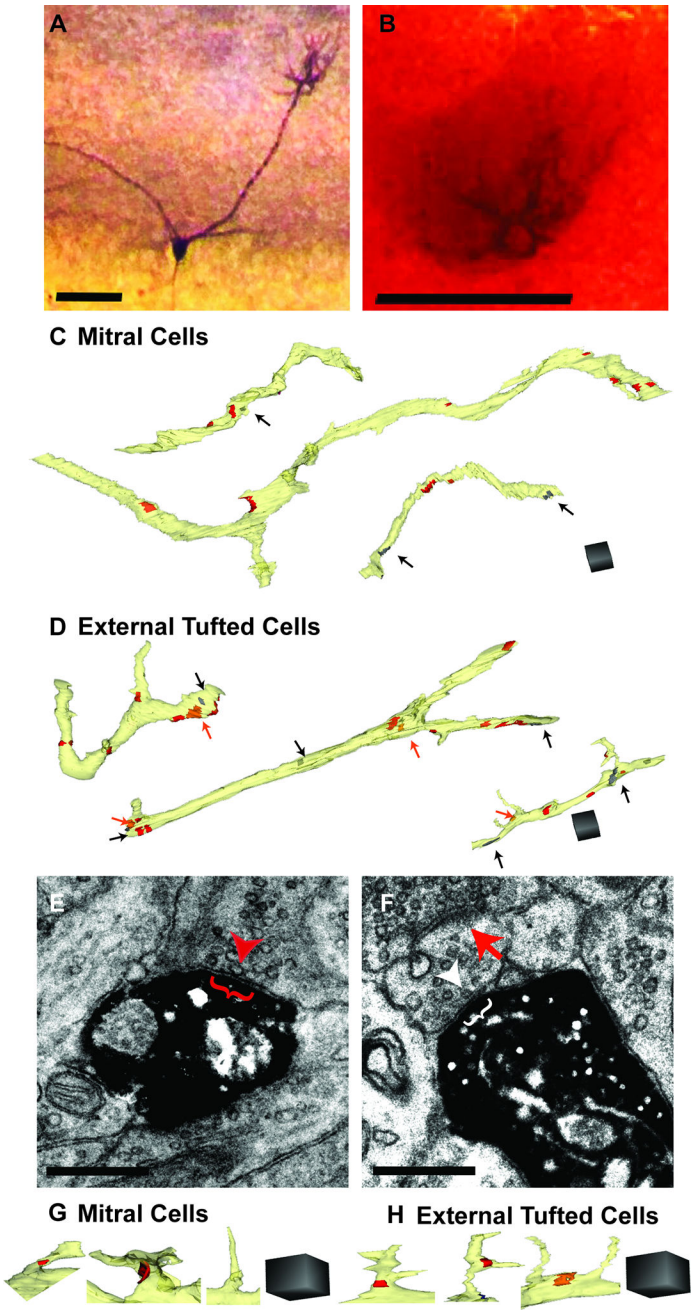

Figure 1. Characterization of apical dendrites of mitral cells (MCs) and external tufted cells (eTCs)

A. Example MC labeled with biocytin following incubation with an avidin-biotin complex and reaction with DAB. Scale bar = 100 μm. **B.** Apical dendritic tuft from same MC shown in Part A after treatment with osmium tetroxide. Scale bar = 100 μm. **C, D.** Example reconstructions of DAB-labeled dendrites (light yellow) of MCs (**C**) and eTCs (**D**). Olfactory sensory neuron (OSN; red) synapses are indicated, as are non-OSN putative excitatory axonal synapses (orange; orange arrows) and putative inhibitory dendrodendritic synapses (gray; black arrows). Scale cubes = 1 μm^3. **E.** Example electron micrograph (EM)

of a DAB-labeled MC dendrite receiving an axo-dendritic synapse from an OSN as indicated by the docked presynaptic vesicles (example at red arrowhead) and active zone (red bracket). Scale bar = 0.5 μm. **F.** Example EM of a DAB-labeled MC dendrite receiving a putative inhibitory dendrodendritic synapse as indicated by docked presynaptic vesicles (example at white arrowhead) and active zone (white bracket). The putative inhibitory dendrite is also receiving an asymmetric axodendritic synapse from an OSN (red arrow). Scale bar = 0.5 μm. **G,H.** Spine-like protrusions with putative excitatory synapses and non-synaptic filopodia-like structures emerging from the dendritic shaft of MCs (**G**) and eTCs (**H**). Scale cube = 1 μm^3.

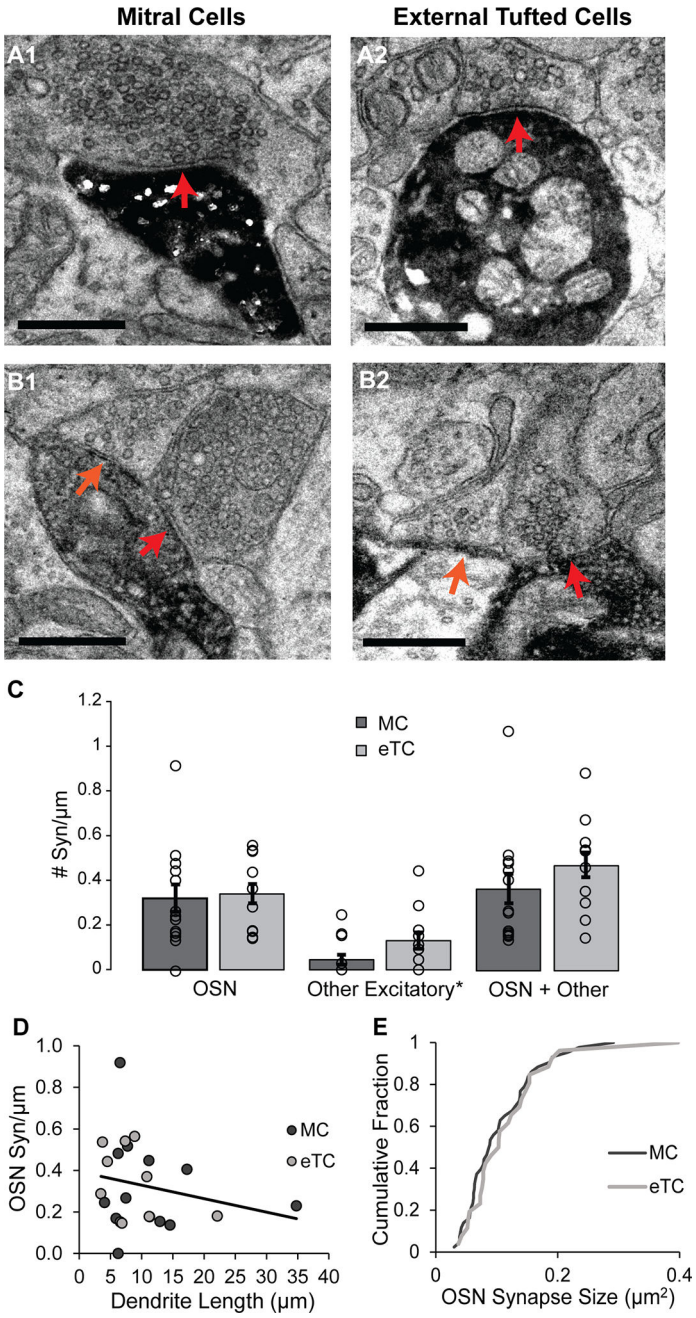

Figure 2. MC and eTC dendrites have similar densities of OSN synapses

A. Examples of OSN synapses onto a MC (A1; red arrow) and eTC (A2), as characterized by docked synaptic vesicles at the presynaptic membrane and the relatively dark appearance of the axon terminal. Scale bar = 0.5 µm. **B.** Unidentified putative excitatory axons (orange arrows) synapse on MCs (B1) and eTCs (B2) next to OSN synapses (red arrows). For the eTC example, the DAB-labeled dendrite extends across the bottom of the image. In the imaged plane, the lighter colored region is a mitochondrion within the dendrite. Scale bar = 0.5 µm. **C.** MC and eTC dendrites have similar densities of both OSN synapses (right), as well as unidentified, putative excitatory axonal synapses (middle). Histogram bars reflect

mean values (±SE); density estimates from each analyzed dendritic segment are also overlaid. Asterisk on “Excitatory” emphasizes putative assignment. **D**. Estimates of OSN synapse densities were independent of the length of the dendritic segments analyzed. R^2 = 0.05. **E.** No difference was also observed in the distributions of OSN synapse size between MCs and eTCs.

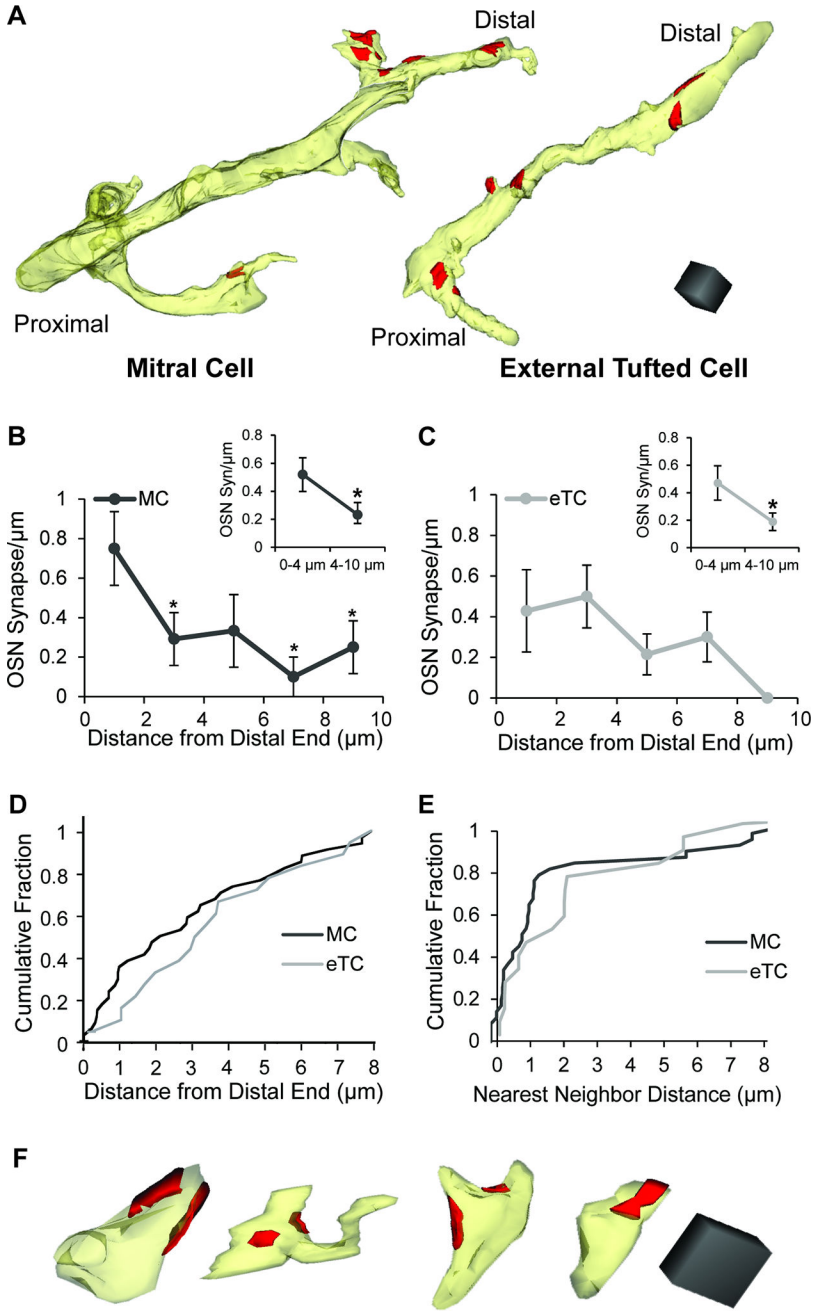

Figure 3. Spatial distribution of OSN synapses on MC and eTC dendrites

A. Reconstructions of a MC and eTC dendrite showing the distribution of OSN synapses (red). Scale cube = 1 µm^3. In these examples, there were no other types of synapses identified. **B.** On MC dendrites, the density of OSN synapses was higher at the distal-most 2 µm of the segments versus more proximal regions. Asterisks reflect significant differences ($p < 0.05$) in OSN synapse densities in the indicated intervals versus 0–2 µm (in pair-wise tests following an ANOVA). This pattern was also observed when the intervals were grouped together (inset; *$p < 0.05$). **C.** OSN synapse density did not significantly vary along eTC dendrites when analyzed in 2-µm intervals, but a distal preference was observed when

intervals were grouped together (inset; *$p < 0.05$). **D**. Cumulative distributions of OSN synapse distances from the distal ends of dendritic segments. The MC and eTC distributions were quite similar (K–S; $p = 0.46$). **E.** Cumulative distributions of distances between nearest neighboring OSN synapses for MCs and eTCs. Note the large number of closely-spaced OSN synapses on MCs, suggestive of clustering. **F.** Reconstructions of terminal ends of MC dendrites, all of which have OSN synapses (red) within 0.5 μm of the tip. Scale cube = 0.125 μm^3.

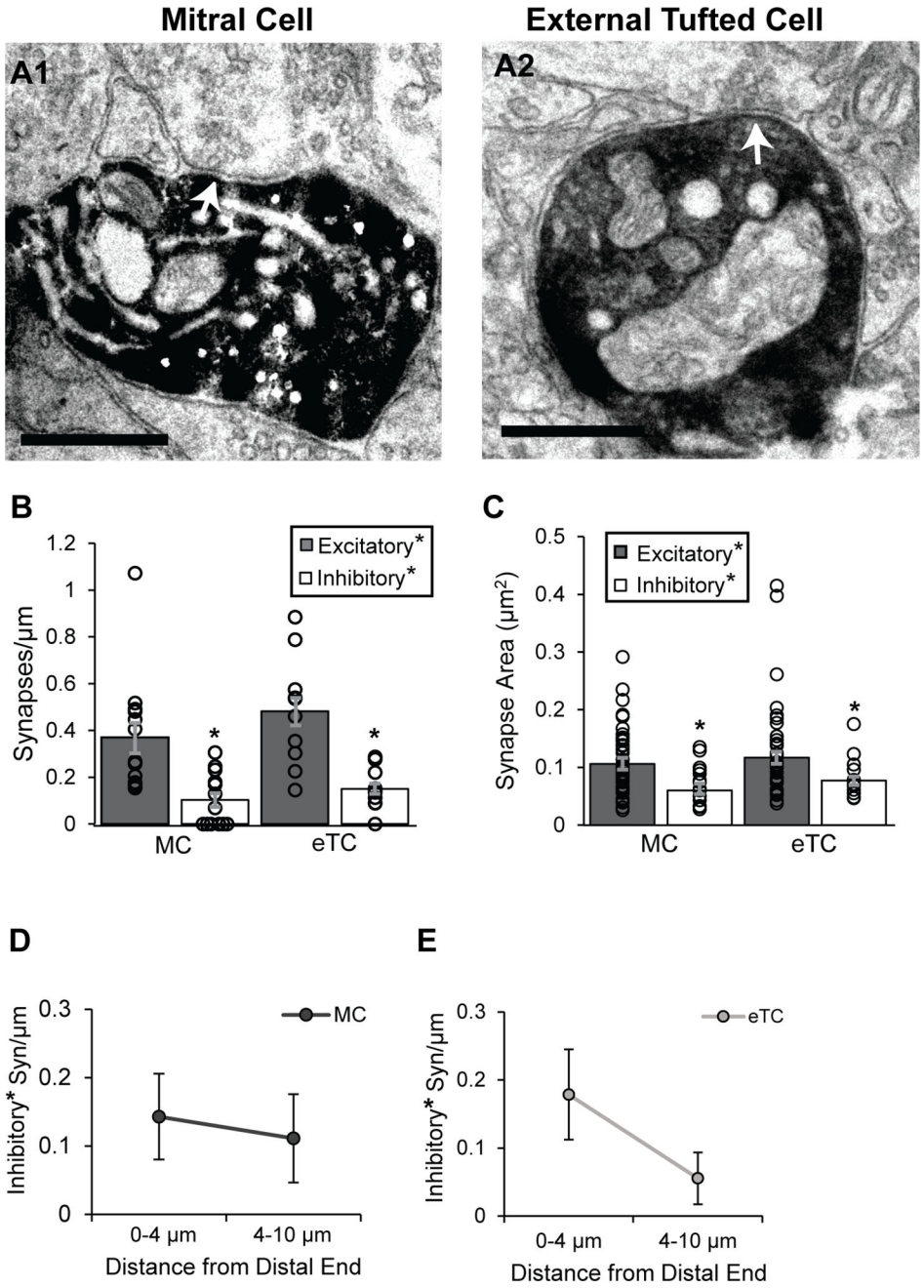

Figure 4. Analysis of putative inhibitory synapses on MCs and eTCs

A. Electron micrographs of putative inhibitory dendrodendritic synapses onto a DAB-labeled MC (A1; white arrow) and eTC (A2). Note the vesicles that appear to be docked at the presynaptic membranes. In these examples, the presynaptic processes were followed to confirm that they formed a symmetric (inhibitory) synapse on an unlabeled dendrite (not shown). Scale bar = 0.5 µm. **B.** In both MCs and eTCs, putative inhibitory synapses (dendrodendritic plus axonal) were much fewer in number than putative excitatory synapses (*$p < 0.05$; all types). At the same time, the two cell-types displayed similar densities of putative inhibitory synapses. Histogram bars reflect mean values (±SE); density estimates

from each analyzed dendrite are also shown overlaid. Asterisks on “Excitatory” and “Inhibitory” emphasize putative assignments. **C.** Putative inhibitory synapses were significantly smaller in size versus putative excitatory synapses on both cell types (*$p < 0.05$). **D,E.** The distribution of putative inhibitory synapses on MCs (**D**) and eTCs (**E**) dendrites did not significantly vary with distance from the distal end.

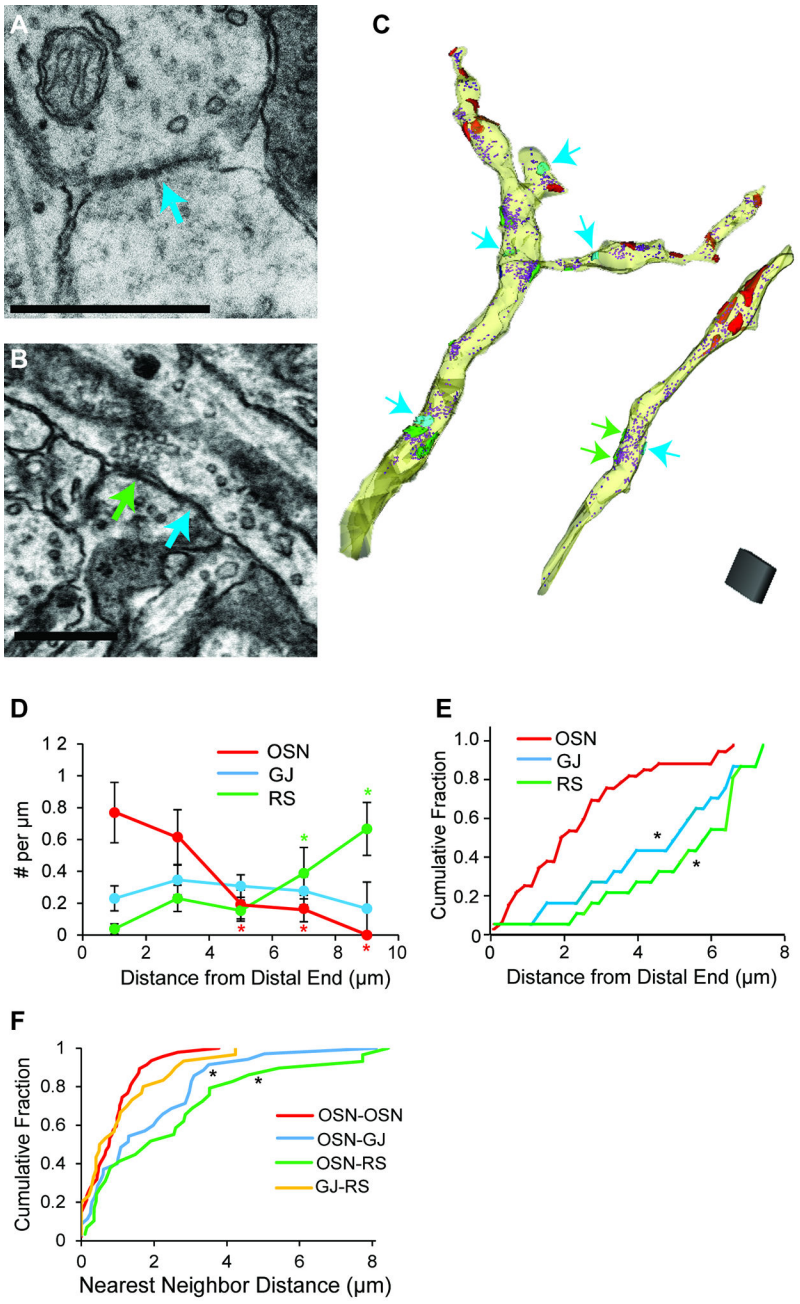

Figure 5. Distribution of OSN synapses, gap junctions, and release sites on unlabeled putative MC dendrites

A. Example of a gap junction (teal arrow) between two unlabeled dendrites. Scale bar = 0.5 µm. **B.** A putative MC dendrite forming a synapse (green arrow) and gap junction (teal arrow) with the same post-synaptic process. The presynaptic putative MC dendrite runs diagonally across the image. Scale bar = 0.5 µm. **C.** Reconstructions of two putative MC dendrites with OSN synapses (red), gap junctions (teal, teal arrows), presynaptic release sites (green), and vesicles (purple). Note examples of release sites that are close to (within ~1 µm of) gap junctions. In the dendrite at right, two release sites across from a gap junction

that are difficult to visualize are indicated with green arrows. Scale cube = 1 μm^3. **D.** Summary of spatial distributions on the distal-proximal axis. Unlike distal-favoring OSN synapses (red), gap junctions (teal) were evenly distributed, while release sites (green) were more highly localized on proximal portions of the dendritic segments. Colored asterisks reflect significant differences ($p < 0.05$) in densities for the indicated intervals versus 0–2 μm (in pair-wise tests following an ANOVA). **E**. Cumulative distributions of distances from the distal ends of putative MC dendrites, plotted for OSN synapses, gap junctions, and presynaptic vesicular release sites. OSN synapses were located more distally than both gap junctions and release sites (K–S: $*p \leq 0.005$), but the positions of gap junctions and release sites were not significantly different (K–S: $p = 0.77$). **F.** Summary of nearest neighbor distances. OSN synapses (red) were clustered together, as were gap junctions with release sites (yellow). OSN-to-gap junction (blue) and OSN-to-release site (green) distances were significantly longer ($*p \leq 0.002$) as compared to OSN synapse-to-OSN synapse distances.

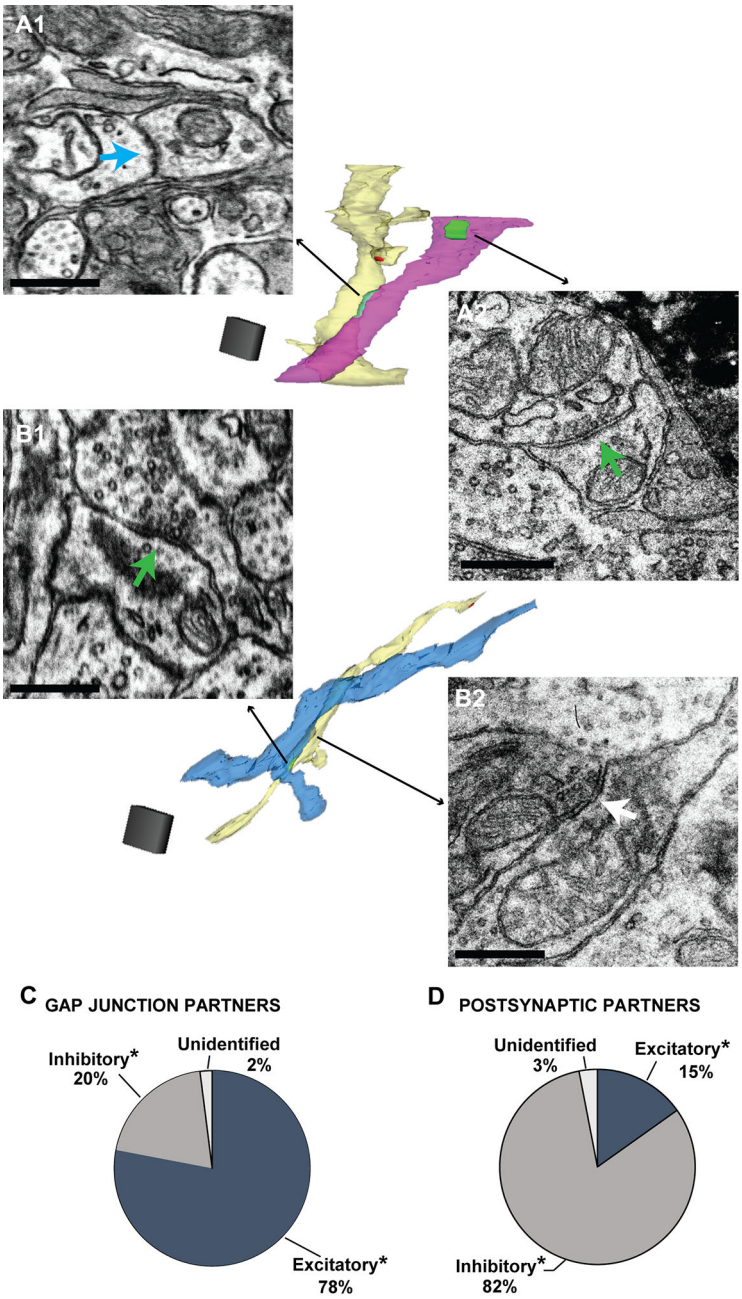

Figure 6. Gap junctional and chemical synaptic partners of putative MC dendrites

A. A putative MC dendrite (light yellow reconstructed dendrite in middle) connected through a gap junction (A1, teal arrow) to a putative excitatory dendrite (pink reconstructed dendrite), as indicated by the asymmetric dendrodendritic synapse (A2, green arrow) onto another process (not shown in image of reconstructed dendrites). Scale bars = 0.5 μm. Scale cube = 1 μm^3. **B**. Putative MC dendrite (light yellow reconstructed dendrite) that formed a putative excitatory chemical synapse (B1, green arrow) onto a putative inhibitory dendrite (blue reconstructed dendrite), as indicated by the symmetric dendrodendritic synapse (B2, white arrow) onto another process (in this case, it was the same putative MC dendrite). Scale

bars = 0.5 μm. Scale cube = 1 μm^3. **C.** Putative MC dendrites formed gap junctions mainly with putative excitatory dendrites. **D.** Putative MC dendrites formed chemical synaptic contacts mainly onto putative inhibitory dendrites.

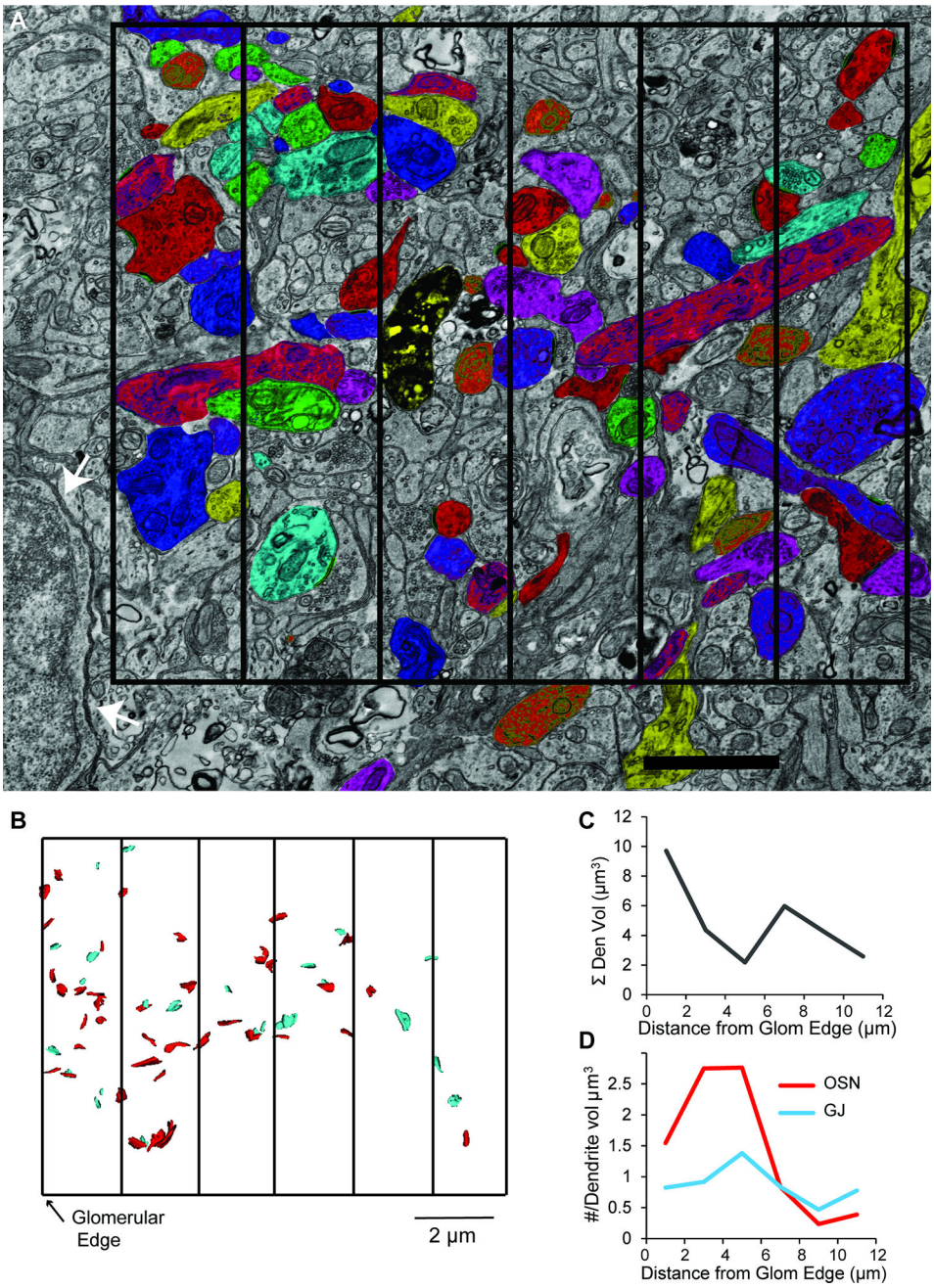

Figure 7. OSN synapse density decreases with distance from the glomerular edge

A. Electron micrograph with a subset of traced dendrites in the glomerular neuropil. The cell bodies of juxtaglomerular cells (example at white arrows) defined the outer edge of the glomerulus. Images were analyzed in 2 × 10 × 2 μm rectangular cuboids. A two-dimensional 12 × 10 μm grid divided into six sections is superimposed, with the left-most vertical line reflecting the edge of the glomerulus. Scale bar = 2 μm **B.** Reconstruction of OSN synapses (red) and gap junctions (teal) from putative MC dendrites across the six rectangular cuboids. **C.** The summed volume of analyzed dendritic segments within each rectangular cuboid plotted as a function of distance from the glomerular edge. Note that the analyzed dendritic

volume was largest within the first 2 μm from the edge. **D.** Densities of OSN synapses (red) and gap junctions (teal) normalized to the volume of dendrite analyzed plotted as a function of distance from the glomerular edge. The density of OSN synapses (red line) was highest close to the glomerular edge, whereas the density of gap junctions (teal line) remained more consistent.